Medical Image Analysis 16 (2012) 675–686

Contents lists available at SciVerse ScienceDirect

Medical Image Analysis

journal homepage: www.elsevier.com/locate/media

Multi-modal registration of speckle-tracked freehand 3D ultrasound to CT in the lumbar spine

Andrew Lang [a], Parvin Mousavi [a,b], Sean Gill [b], Gabor Fichtinger [a,b,c,d], Purang Abolmaesumi [b,e,*]

[a] Department of Electrical and Computer Engineering, Queen's University, Kingston, Ontario, Canada
[b] School of Computing, Queen's University, Kingston, Ontario, Canada
[c] Department of Mechanical and Materials Engineering, Queen's University, Kingston, Ontario, Canada
[d] Department of Surgery, Queen's University, Kingston, Ontario, Canada
[e] Department of Electrical and Computer Engineering, University of British Columbia, Vancouver, British Columbia, Canada

ARTICLE INFO

Article history:
Available online 27 August 2011

Keywords:
Freehand ultrasound
Speckle tracking
Registration
Image-guided intervention
Drift correction

ABSTRACT

A method for registration of speckle-tracked freehand 3D ultrasound (US) to preoperative CT volumes of the spine is proposed. We register the US volume to the CT volume by creating individual US "sub-volumes", each consisting of a small section of the entire US volume. The registration proceeds incrementally from the beginning of the US volume to the end, registering every sub-volume, where each sub-volume contains overlapping images with the previous sub-volume. Each registration is performed by generating simulated US images from the CT volume. As a by-product of our registration, the significant drift error common in speckle-tracked US volumes is corrected for. Results are validated through a phantom study of plastic spine phantoms created from clinical patient CT data as well as an animal study using a lamb cadaver. Results demonstrate that we were able to successfully register a speckle-tracked US volume to CT volume in four out of five phantoms with a success rate of greater than 98%. The final error of the registered US volumes decreases by over 50 percent from the speckle tracking error to consistently below 3 mm. Studies on the lamb cadaver showed a mean registration error consistently below 2 mm.

1. Introduction

Lower back pain is a prevalent problem which can be treated through spinal injections at the facet joint (Datta et al., 2009). These injections are often performed under CT or fluoroscopic guidance. Image-based guidance assists in achieving desired clinical accuracy and precision requirements of the procedure. The drawbacks of using CT and fluoroscopic guidance include high costs and exposure of both the patient and surgeon to ionizing radiation. A possible approach to alleviate these issues is to use ultrasound (US) guidance for spinal injections, in particular, facet joint injections.

Unfortunately, US guidance alone proves to be challenging due to the difficulty in interpreting US images in the spine region. Additionally, the bony structure of the spine produces shadowing in the US image, possibly occluding the injection site. Therefore, a preoperative image such as a CT scan could be employed to aid in intraoperative US guided spinal injections. After the initial CT scan is taken, a preoperative plan can be developed to define the target area for injection. Registration of this preoperative CT to the intraoperative US allows the location of the US images to be known relative to the targeted CT region. In such a multimodal procedure, care must be taken to register the CT and US images to a common coordinate frame. Registration of a single 2D US image is not sufficient; therefore, 3D US is required for guidance. The target area for a facet joint injection is approximately 1.5 cm in diameter. Given the size of the target, surgical practice requirements call for about 3 mm accuracy, a sufficiently close distance to envelop a nerve sack in anesthetic agent. It is worth noting that for this procedure, pinpoint accuracy may not be necessary. Similar clinical outcome is achieved with small targeting errors as long as the injected drug diffuses into the facet joint.

In the literature, many US-to-CT registration approaches have been previously proposed. These include both feature-based and intensity-based techniques. In feature-based registration techniques, it is common to register segmented bone surfaces from both the CT and US volumes using a variation of the iterative closest point (ICP) technique (Besl and McKay, 1992). The biggest drawback with the feature-based methods is the need to segment the bone surfaces in US. Noisy US images and the shadowing below bone surfaces makes automatic bone segmentation difficult. Sev-

* Corresponding author at: Department of Electrical and Computer Engineering, University of British Columbia, 2332 Main Mall, Vancouver, BC, Canada V6T 1Z4. Tel.: +1 604 827 4741; fax: +1 604 822 5949.
E-mail address: purang@ece.ubc.ca (P. Abolmaesumi).

1361-8415/$ - see front matter © 2011 Elsevier B.V. All rights reserved.
doi:10.1016/j.media.2011.07.006

eral examples of feature-based registration methods for CT and US volumes containing bone structures, are reported in the literature. Among these methods, Herring et al. (1998) used ICP to register surface points of the spine extracted from the US and CT images. US surface points were extracted using a combination of morphological operations, linear thresholding and ray-tracing. CT points were found manually. Experimental results were performed using an untracked US probe that imaged a plastic spine phantom placed in a water tank, and thus quantitative accuracy results were not available. Building on this, Muratore et al. (2002) registered US and CT images of the lumbar vertebrae using ICP; however, CT surface points were extracted using a modified Marching Cubes algorithm. Barratt et al. (2005) proposed using a point-based registration method between CT and US that simultaneously determined the calibration parameters for the freehand 3D US system. Manual segmentation was used to define the surface points. Finally, Moghari and Abolmaesumi (2005) proposed an improved registration framework replacing the ICP registration with an unscented Kalman filter based method. Results were reported on manually segmented US surface points. While feature-based registration of US and CT images shows promise with acceptably low reported error values, it relies significantly on the accuracy of the segmentation of the surface points. In many cases, these points are determined manually as automatic surface point extraction in US images is difficult to perform.

Among intensity-based registration methods for CT and US volumes containing bone structures, Winter et al. (2008) proposed a surface-volume registration framework between extracted bone-surface points from CT data and a US volume that has bone surfaces enhanced via processing. Penney et al. (2006) converted both the CT and US volumes into probability images before calculating the similarity. A value representing the probability of a pixel being a bone–tissue interface is created for the CT and US images. Using another approach to US-to-CT registration, Wein et al. (2008) generated a simulated US volume from the CT volume, leading to a more closely matched registration problem. Density information in the CT was used as a simple approximation to acoustic impedance for generating simulated US images. Later, Shams et al. (2008) extended this approach to include beam width effects and speckle noise. Recently, Gill et al. (2009a) proposed a method for registration of a preoperative CT volume to a 3D US volume for the lumbar spine. They used a groupwise approach to register the L3 to L5 vertebrae allowing unconstrained free motion between them. A biomechanical model was later introduced to restrain the motion of these vertebrae in a more realistic clinical representation (Gill et al., 2009b). A potential drawback to image-based registration methods is that they generally require a more accurate initial alignment than feature-based methods. It is thereby important to analyze the capture range of the registration, or the maximum amount of initial misalignment resulting in a successful registration.

Many of the above mentioned approaches use freehand tracked 2D US to generate 3D US volumes for use in registration. As opposed to using a 3D US probe, using a 2D US probe to generate 3D volumes has the advantages of lower cost, smaller size, higher image resolution, and the ability to generate arbitrarily large extended field-of-view volumes. In the case of spine imaging, the ability to generate volumes consisting of several vertebrae is very important. For the majority of spinal injections, palpation of the iliac crest, the C7 vertebrae, or the twelfth rib, followed by counting the vertebrae level from those anatomical landmarks determines the puncture site. Freehand 3D US allows for the conversion of 2D US images into a 3D US volume provided that a reliable tracking method for the probe can be used (Fenster et al., 2001). Unfortunately, this tracking is sometimes cumbersome, preventing widespread use of 2D US to generate 3D volumes for clinical purposes. Traditionally, tracking of the US probe is done using optical or electromagnetic tracking. Speckle tracking has been proposed as an alternative method for generating freehand 3D US reconstructions (Weng et al., 1997; Tuthill et al., 1998). With the limited availability of tracking technology for use in clinical cases, speckle-tracked 3D US provides a desirable and inexpensive choice.

In speckle tracking, the amount of correlation between subsequent US images is used to determine the inter-frame spacing. While this approach has the advantage of not requiring any external tracking device in the procedure room, it has been shown to exhibit rather poor accuracy with significant rotational and translational drift errors. Advanced methods proposed in the literature have been shown to reduce these inaccuracies (Housden et al., 2007; Laporte and Arbel, 2008; Rivaz et al., 2007). Housden et al. (2007) developed a comprehensive 3D speckle-tracked reconstruction algorithm in which US inter-frame spacing, frame intersections, and non-monotonic elevational motion of the US probe are taken into account. Laporte and Arbel (2008) extended this work by incorporating a probabilistic model for elevational motion. Multiple correlation measurements ares then placed into a Maximum Likelihood Estimation framework. Rivaz et al. (2007) attempted to detect the fully-developed speckle (FDS) within the US images based on the statistics of the noise. The regions of detected FDS can be irregularly spaced throughout each US image. Despite all of these methods, drift errors associated with speckle tracking can never be completely eliminated, only reduced. Other areas of research related to improving the accuracy of speckle tracking include the fusion of speckle tracking with a secondary tracking system (Housden et al., 2008a,b; Lang et al., 2009). However, there have been no cases of using speckle-tracked 3D US in an image registration framework.

To accurately incorporate speckle-tracked 3D US into a US-to-CT registration framework, it is necessary to correct for the significant drift errors. Correction for these errors would lead to the possibility of speckle tracking being a useful tool for image based guidance. Drift correction requires positional information that, in the case of registration, can be obtained from the CT volume itself. Modification of the US-to-CT registration framework to incorporate drift correction is necessary. The clinical framework for facet joint injections, our selected application for incorporation of speckle-tracked 3D US, would be changed minimally as a result of such incorporation. An initial speckle-tracked volume is acquired of the spine, after which a drift correcting registration routine is used to generate a more accurate reconstruction. All subsequent US images are then registered to this drift corrected volume within a US-to-US registration framework.

In this work, we propose a method for the registration of speckle-tracked 3D US to CT by incrementally registering sub-volumes of a full speckle-tracked US volume, while simultaneously correcting for the drift in the volume. While speckle tracking for 3D reconstruction of US data has been proposed before, many algorithms show substantial 3D reconstruction error over a long scanning range. This has hindered the clinical applicability of such techniques. We therefore explore the feasibility of using a US-to-CT registration framework to compensate for the drift error of a speckle-tracked US reconstruction. We validate our work through a phantom study of plastic spine phantoms created from clinical patient CT data as well as an animal study using a lamb cadaver.

This paper is organized as follows. Section 2 discusses the methodology of our registration framework. Section 3 presents the results of our methods when applied to spine phantom images and the animal cadaver. In Section 4 we discuss the results and finally in Section 5, we present concluding remarks.

2. Methods and materials

Our aim is to register a speckle-tracked freehand 3D US volume to a preoperative CT volume. Due to the poor accuracy of the

speckle-tracked volume, we cannot register the entire speckle-tracked US volume directly to the CT volume. Instead, the proposed registration works on "sub-volumes" of the entire US volume. The overview of our registration framework is presented in Fig. 1. During registration, the entire CT volume is considered as the "fixed image" while the US sub-volume is considered as a "moving image" and thus is transformed into the coordinate system of the CT volume. In this multi-slice-to-volume framework, an optimization is carried out to determine the best transformation between the US sub-volume and the CT volume. Sub-volumes are registered to the CT volume in a successive fashion with overlap between each sub-volume.

2.1. Methods

2.1.1. Speckle tracking

The US images being acquired and used consist of the envelope-detected radio frequency (RF) data. Speckle-tracked reconstruction requires that the US intensity signal is used and therefore, processed B-mode US images cannot be used (Chen et al., 1997). Upon acquisition of two or more individual freehand 2D US images, an initial speckle-tracked 3D volume is generated. As each new US image is acquired, its placement in the volume is determined relative to the previous frame, provided sufficient speckle correlation exists between the two images. Since no external tracking is used, the coordinate system of the overall volume is arbitrarily defined to be the origin of the first US image in the acquired sequence. The methods for finding the position of a single frame relative to a previous frame follow a simplified version of the work of Housden et al. (2007). For our experiments, each acquired US frame is divided into an 8×7 grid of patches or blocks (Fig. 2a). This grid size was empirically found to work well for the size of our data. Three in-plane and three out-of-plane transformation parameters between the two frames are determined. These parameters, t_x, t_y, t_z, θ_x, θ_y and θ_z, represent the three translations and three rotations. Image patches containing areas of noise, bone and shadow are also excluded from the calculation of the transformation parameters. Finally, the overall speckle-tracked 3D US reconstruction is updated based on the position of the current frame.

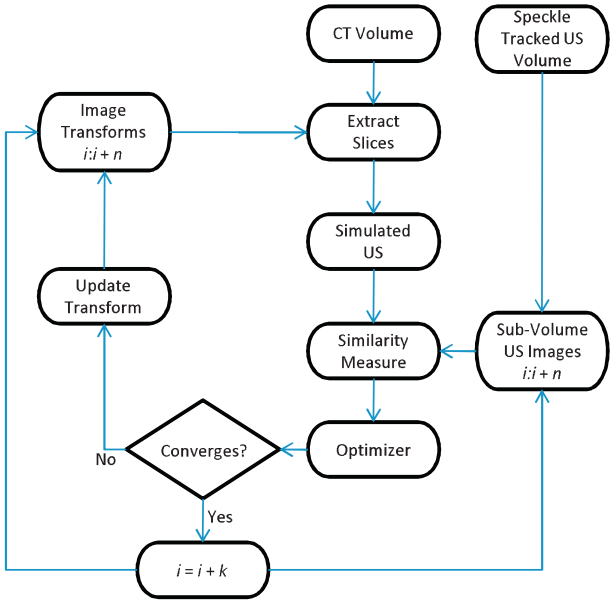

Fig. 1. Overview of the registration framework where i is the starting frame of the current sub-volume, n is the number of frames in each sub-volume, and k is the number of frames to skip after each sub-volume registration.

2.1.1.1. Estimation of in-plane parameters. The in-plane parameters, t_x, t_y and θ_z are solved for as in an image registration problem. A block matching method is employed as devised by Housden et al. (2006). Each image block is registered in two images based on the maximum value of the normalized cross-correlation (NCC) metric. Sub-pixel translations are estimated for each block by fitting a Gaussian function to the neighborhood of NCC values surrounding the maximum value. After determining the x and y translations for each block, the in-plane parameters between the two images are then determined by a least-squares best fit of the translation vectors using a 2D version of the technique of Arun et al. (1987).

2.1.1.2. Estimation of out-of-plane parameters. The heart of the speckle-tracked reconstruction method is in the estimation of the out-of-plane parameters between each image. To do this, we take advantage of the 3D nature of the US beam. Speckle decorrelation curves of the type in Fig. 2b are created so that the relationship between the NCC value and the separation distance is known. A distinct correlation curve is created for each image block. The curves were determined by rigidly mounting the US probe above a speckle phantom such that the probe surface was completely parallel to the phantom surface. A speckle phantom was placed on a linear stage with micron accuracy, which then moved in 0.02 mm increments up to 2 mm. Given the known distance between each image, the speckle decorrelation curves were created for each block by

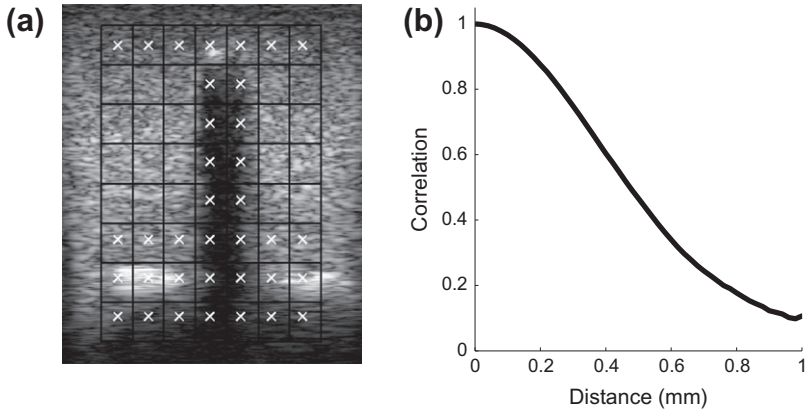

Fig. 2. (a) For speckle tracking, each image must first be divided into a grid of blocks. Blocks not included are marked with a white 'x'. (b) An example of a decorrelation curve that relates the correlation value to a distance.

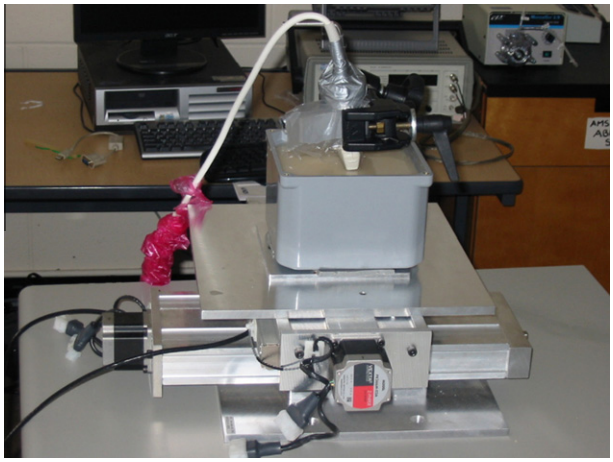

Fig. 3. A look at the stage setup used to accurately measure the distance between US frames so that the decorrelation curves could be created. The US probe is rigidly mounted to a table while the stage moves the speckle phantom below it. The probe is mounted such that the image is approximately perpendicular to the surface of the phantom.

calculating the NCC value between the image blocks. Fig. 3 shows the experimental setup for acquiring the decorrelation curves.

With pre-calculated decorrelation curves, the out-of-plane elevational translation for each image block is determined using the NCC value calculated previously for the estimation of the in-plane parameters. The decorrelation curves act as a series of look-up tables. Provided the distance is known between all of the blocks on an image, a plane is fit using a least-squares method to solve the equation of a plane (Krupa et al., 2007).

2.1.1.3. Exclusion of no-speckle areas. It is very important that only patches containing speckle are used, so as to not affect the speckle tracking accuracy by degrading speckle correlation. Therefore, any patches containing either a strong bone reflection or the underlying shadow below the bone are discarded. Additionally, the first row and the last three rows in each image are excluded due to the poor elevational focusing and excessive noise exhibited in these areas. An example of the excluded blocks can be seen in Fig. 2a, with the excluded blocks marked by a white 'x'.

Blocks containing bone or shadow can be fairly simply determined automatically through analysis of each block's histogram. We first take the square root of each pixel in the RF US frame to reduce the dynamic range of pixel values. Next, to find areas of shadow, a threshold value for the shadow intensity is chosen along with a corresponding threshold for the percentage of shadow pixels in the block. The percentage of total pixels with values *below* the given intensity threshold is then calculated. If this percentage is above the chosen percentage threshold, then the block is determined to be a likely area of shadow. Based on empirical observation, for an image intensity range of 0–255, values of 22 for the intensity threshold and 35 for the percentage threshold were used for our images. The same thresholding technique can be used to find bright bone surface reflection blocks. In this case, the percentage of total pixels with values *above* the given intensity threshold are calculated and compared to the chosen percentage threshold. Again, if the calculated percentage is above the percentage threshold, then the block is said to be an area with strong reflections. Values of 90 for the intensity threshold and 15 for the percentage threshold were used in this case. All of the given values are entirely dependent on the gain levels of the US system. While fixed thresholds are not an ideal solution to determining areas of bone and reflection in the images, they work well enough for the problem at hand. Throughout our experiments, these threshold values remained constant, as did the US settings. When moving to a clinical setting in future research, there will be a need to optimize for these parameters or include a more robust approach for identification of high reflection and shadow regions in the images.

2.1.1.4. Correction for real tissue. When real tissue is scanned with US, a minor adjustment in the speckle-tracking algorithm must be made. In US images, real tissue will not always contain fully developed speckle (FDS) because of the addition of ligaments, muscle and fat (Hassenpflug et al., 2005). In our own experiments, we deal with both speckle phantoms and lamb spine tissue. For the speckle-tracked US reconstructions of the lamb spine, this lack of FDS is corrected for. The method that we use to correct for a lack of FDS was developed by Gee et al. (2006). The general idea of this method is that the speckle decorrelation model (Fig. 2b) for each block is modified to account for the coherent components within the speckle. An estimation of this coherency is determined by using the decorrelation curves in the axial and lateral directions.

2.1.1.5. Speckle-tracked reconstruction. The complete speckle-tracked reconstruction is created by starting with the first frame of the sequence. The next frame in the sequence is determined to be the frame that is at the optimal distance from the first frame, as estimated by the speckle tracking (Housden et al., 2007). Any frame estimated to be at a distance closer than this value is discarded. We used a value of $d = 0.3$ mm as the optimal distance which gave the best results. This value was chosen as it is close to the average mid-point of the speckle decorrelation curves for each block and has been shown to be a reasonable distance for speckle tracking accuracy (Hassenpflug et al., 2005). Frames continue to be selected in this fashion throughout the sequence. Provided no optimally spaced frame exists, the frame closest to the optimal distance is chosen as the next frame. Important differences between our reconstruction and that of Housden et al. (2007) are that only a single speckle-tracked reconstruction is generated and acquired US frames are assumed to be monotonic and non-intersecting. For the purposes of our work, the US probe scan direction is assumed to be in one single monotonic direction along the spine.

It should also be noted that a complete loss of speckle correlation is possible and likely to happen in any given freehand sweep. This loss can happen for a variety of reasons such as hand tremor and patient motion. To compensate for cases where correlation is lost, a semi-linear probe motion is assumed. If correlation is lost for only a few frames, the linear probe motion assumption means that the probe position can be extrapolated linearly based on the previous probe motions. Additionally, the registration method that will be presented in Section 2.1.3 is able to correct for this temporary problem. Any significant patient or probe motions should however be detected by the clinician and may require restarting the US imaging process.

Upon the final selection of frames for reconstruction, the RF US data is converted into B-scan data via log compression and scan-conversion to improve the visual quality of the US images for the registration procedure. First, the RF US data is compressed using a compression table created with the following equation

$$c = \frac{e^{\alpha \log x}}{e^{\alpha \log 2^{14}}/255.0} \tag{1}$$

where c is the compression value for a given RF US value, x, and x is a 14-bit number in our case. The value of α is set to 0.14. The post-compression image is then resized to a more reasonable size, converting the x and y pixel scale to 0.13 mm/pixel using bicubic interpolation. This value is the default scale used by our US machine

for B-scan images. Next, contrast adjustment is performed to enhance the contrast between bone shadows and the surrounding tissue. Here, the intensity values in the range between 110 and 255 are remapped to the range between 0 and 255. Finally, a gamma correction is applied to adjust the brightness of the final image, using $\gamma = 1.66$.

2.1.2. Ultrasound simulation

As outlined in Fig. 1, at each iteration of the registration framework, the slices extracted from the CT volume are transformed to a new position, with the purpose of finding the transformation leading to maximum similarity between the CT and US volumes. This transformation takes place before the similarity measure is calculated. Since a multi-slice-to-volume technique is being employed, multiple 2D slices must first be extracted from the CT volume, each one corresponding to the position of a 2D freehand US slice. To increase the similarity between the CT slices and the US images, the CT slices are processed into simulated US images. Following the method of Wein et al. (2008), the US simulation takes three steps: (1) the simulation of the US reflection from CT, (2) mapping the CT values to those found in US, and (3) calculating the weights to combine these two images with a bias correction term. Additionally, bony structures in the image are masked out as were performed by Gill et al. (2009a), where the threshold for full reflection was set to $\tau = 150$. Gradient values above this threshold signify a bone edge, forcing the US transmission beyond that point to zero.

We made two modifications to the US simulation method of Wein et al. (2008) and Gill et al. (2009a). The first is that any time the τ threshold is met in the reflection image, a value equal to the maximum intensity in the US image is assigned to the final simulated US image. As bone produces a very strong reflection at bone–tissue interfaces, this mapping helps to identify bone surfaces. The second addition is that we consider all pixels with intensity value below 10 as one single shadow region, with its own weights calculated from step (3) above. This intensity value was chosen as the average intensity within the shadow regions our ultrasound data sets.

2.1.3. CT to speckle-tracked US registration

As previously mentioned, speckle tracking suffers from a significant amount of drift. Drift causes the reconstructed US volume to be substantially misaligned from the CT data. This misalignment cannot be completely corrected for by a rigid registration between the two volumes. Therefore, a straightforward registration framework, such as those used in Wein et al. (2008) and Gill et al. (2009a), is not sufficient.

In our registration algorithm, as shown in Fig. 1, we divide the registration problem into a series of smaller rigid registrations. It has been shown that over a short scan distance, speckle-tracked 3D US yields a reasonably accurate US volume (Housden et al., 2008a). Therefore, it is logical to use a series of sub-volumes of speckle-tracked US in our registration. The first sub-volume is taken from the first n US frames. This sub-volume is subsequently rigidly registered to the entire CT volume (Gill et al., 2009a). A standard image registration framework is used to find the best transformation, $\widehat{\mathbf{T}}$, that maps the CT volume position to that of US volume in which the optimization approach is used:

$$\widehat{\mathbf{T}} = \arg\max_{\mathbf{T}}(S(\mathrm{US}(x), \mathrm{CT}(\mathbf{T}(x))) - \alpha R(\mathbf{T})) \tag{2}$$

where US (x) is the US sub-volume, CT (x) is the CT volume, $\mathbf{T}(x)$ are the transformed CT voxel positions, $S(I_1,I_2)$ is the similarity measure between two images and $R(\mathbf{T})$ is a regularization function scaled by α used to limit the movement of each sub-volume. The similarity measure is defined by the Linear Correlation of Linear Combination (LC^2) metric (Wein et al., 2008):

$$\mathrm{LC}^2 = \frac{\sum_{x,y}(\mathrm{US}(x,y) - f(x,y))^2}{P \times Var(\mathrm{US}(x,y))} \tag{3}$$

where P is the number of pixels that overlap between the CT and US images and $f(x, y)$ is the simulated US image created from the CT volume after slice extraction based on the position of each US frame. Finally, since we are using a multi-slice-to-volume framework, the LC^2 measure is averaged over all slices in the US sub-volume.

The Covariance Matrix Adaptation Evolution Strategy (CMA-ES) (Hansen, 2006) is used to optimize the transformation, $\mathbf{T}$, that transforms the US coordinate system to the CT coordinate system. Upon completing this initial sub-volume registration, the final transformation, $\widehat{\mathbf{T}}_{1:1+n}$, is applied to the entire volume, or frames 1 to N, where N is the number of frames per US volume. The next sub-volume is chosen such that it overlaps the previous sub-volume, only offset by k number of frames. Therefore, US frames $1 + k{:}1 + k + n$ are chosen to create the next US sub-volume to be registered to the CT volume. The resulting transformation, $\widehat{\mathbf{T}}_{1+k:1+k+n}$, will then be applied to all subsequent frames beginning with first frame of the sub-volume, or frames $1 + k$ to N. As such, the full registration process proceeds in a "sliding window" type of fashion, which assures smoothness in the final US registration volume after all sub-volumes are registered.

The value of k must be carefully selected; if k is too small as compared to n, the registration error may increase due to a preference towards the beginning of each sub-volume registration as the leading frames leave the sliding window. Also, if k is too large as compared to n, it may result in an exceedingly "disjoint" registration, where each sub-volume will be more independent of other sub-volumes. A value of k balanced between 1 and n should produce the most accurate registration. Unfortunately, the resulting registration can still be rather jagged due to each sub-volume not completely overlapping the previous sub-volume.

Additionally, the regularization term, $R(T)$, in Eq. (2) is utilized to prevent each individual sub-volume from registering too far from the previous sub-volume, thus preventing outliers in the registration and also ensuring additional smoothness in the resulting volume. The equation for this term is

$$R(\mathbf{T}) = \frac{1}{4}\sum_{i=1}^{4} \|p'_{i,1} - \mathbf{T}(p_{i,1})\|, \tag{4}$$

where $\mathbf{T}(p_{i,1})$ are each of the four corner points from the first frame in the current US sub-volume transformed by the current optimizer transformation, $\mathbf{T}$, and $p'_{i,1}$ are each of the same four corner points as transformed by the previous sub-volume registration. The average Euclidean distance between these two sets of points is used as our regularization term. Thus, we penalize any movement of the sub-volume during registration. A value of $\alpha = 0.01$ was used in our registrations.

2.2. Materials

A Sonix RP ultrasound machine (Ultrasonix Medical Corp., Richmond, Canada) was used to collect RF US frames using an L14-5/38 linear array transducer. An RF frame contained 128 lines with 2064 samples each, with each line subsequently passed through a Hilbert transformation envelope detector. US frames were captured at a depth of 5.5 cm with a probe frequency of 6.6 MHz using a single focal point at 2 cm. Freehand tracking was performed using an optical tracker (Optotrak Certus, Northern Digital Inc., Waterloo, Canada) with a dynamic reference body (DRB) (Traxtal Technologies Inc., Toronto, Canada) rigidly mounted to the probe. The

tracker has a stated accuracy of 0.1 mm. Probe calibration was performed using an N-wire fiducial phantom (Chen et al., 2006). Registrations were run on a Dell Precision 690 with 2 × 2.33 GHz Intel Xeon Quad-core CPU and 16 GB of RAM.

2.2.1. Phantom study

Five tissue mimicking phantoms were created by first segmenting the L1 to L5 vertebrae in five patient CT data sets using ITK-SNAP (Yushkevich et al., 2006). The CT data was collected at Kingston General Hospital and all the patients gave informed consent for this data to be used in our research. The segmented CT images were then used to generate a 3D physical model of lumbar vertebrae using a Dimension SST 3D printer (Stratasys, Inc., Eden Prairie, MN, USA). The natural curvature of the spine is maintained between the patient CT and the printed model. The hard plastic printed vertebrae were securely glued in a plastic container and then filled with a tissue mimicking material (Madsen et al., 2005). The tissue mimicking material was made from a recipe of 1.17% agar (A9799, Sigma–Aldrich, St. Louis, MO, USA), 3.60% gelatin (G9382, Sigma–Aldrich), 1% Germall® Plus (International Specialty products, Wayne, New Jersey, USA) as a preservative, 3% cellulose (S5504, Sigma–Aldrich) for speckle, and 3.2% glycerol (G6279, Sigma–Aldrich) to adjust the speed of sound to approximately 1540 m/s.

Next, 10 CT-visible fiducial markers (Beekley Corp., Bristol, CT, USA) were placed at various locations on the outside of the phantom container and the phantoms were CT scanned at high resolution (0.46 mm × 0.46 mm × 0.625 mm). The locations of the fiducial markers were determined using an optically tracked pointer and the same Certus camera system described before.

2.2.2. Animal study

The spine of a lamb cadaver was also used for evaluation of our technique. Lamb was chosen due to its similarity to that of the human spine. Each vertebra is somewhat smaller; however, there is not as much fat tissue as in other available animal models, such as pig. The lamb spine was rigidly fixed in a box. CT-visible fiducials were then placed on the skin of the lamb surrounding the spine on both sides.

3. Experiments and results

3.1. Phantom study

An initial guess for the gold standard transformation between the US coordinate system and the CT coordinate system was determined through the point-to-point registration technique of Arun et al. (1987). This initial guess was used to determine the final gold standard transformation by rigidly registering each optically-tracked freehand US volume to the CT volume using the previously described method of US simulation. The initial fiducial-based registration was not used as a gold standard in an attempt to remove some of the systematic errors involved with the registration. The major sources of these errors include the US calibration and speed of sound differences.

3.1.1. Speckle tracking and US-to-CT registration

A single freehand 3D US scan was captured from each of the five phantoms consisting of between 295 and 300 frames per volume. The speckle-tracked US reconstruction approach from Section 2.1.1 was performed on each US data set. The resulting speckle-tracked reconstructions contain US frames that are positioned in a coordinate system that is originated at the first frame in the sequence. To transform this volume to the CT coordinate system, it must first be aligned with the optical tracker coordinate system. This alignment can be achieved by simply giving the first frame in the speckle-tracked volume the same transformation as the first frame in the optically tracked volume. This initial transformation is then applied to all subsequent frames in the speckle-tracked volume. Aligning the two US volumes this way allows speckle tracking to be directly evaluated relative to the optically tracked ground truth.

To evaluate the accuracy of speckle-tracked US reconstruction relative to the ground truth optically tracked reconstruction, we analyze the target registration error (TRE) (Fitzpatrick et al., 1998) at each frame in the reconstruction, since each frame is positioned independently of all other frames, and therefore will have a different amount of error. The TRE for a single speckle-tracked US frame is defined as the average Euclidean distance between the four corners of the speckle-tracked image to their respective ground truth positions. The resulting plots of TRE vs. frame number for each of the five speckle-tracked reconstructions are shown in Fig. 4a–e as the lighter colored points. A very clear drift in the error is seen in these plots, with the error beginning at 0 and ending up between 6.4 mm and 10.9 mm.

To test the accuracy of the proposed reconstruction technique, each speckle-tracked US reconstruction was initially aligned to the CT volume using the gold-standard transformation. Clearly, the initial aligned position for the speckle-tracked volume is only in perfect alignment for the first frame, as all subsequent frames drift as previously seen. This US volume was then registered to the CT scan volume from its initial aligned position using the proposed CT to US registration algorithm. These experiments were intended to demonstrate how well the proposed registration method corrects for the drift in the volume. We repeated these registrations of the patient phantoms a total of 100 times each. Each of these 100 trials begins with the US volume at the same location; however, since the CMA-ES optimizer is a randomized method, it is not guaranteed to converge to the same point each time. The results of these registrations can be found in Table 1. Fig. 4a–e displays the plots of the resulting TREs for five example registrations from each of the five patients phantoms as black points. There is a very clear improvement between the speckle-tracked reconstruction error and the registration error, including the elimination of the drift error. Additionally, for visual inspection, overlapping images from the CT scan and the respective ground truth, speckle-tracked and registered US reconstructions can be seen in Fig. 5a–c, where the registered volume is in a very similar position to that of the ground truth.

3.1.2. Registration capture range

For our second set of phantom experiments, we analyzed the capture range of the proposed registration method. For each patient phantom, the speckled tracked US reconstruction in initial alignment with the first frame of the gold standard reconstruction was randomly transformed to a position away from this gold standard position. Transformations were randomly generated using a uniform distribution ranging between ± 5 mm in translation and ±5° in rotation, and used to produce a pseudo-uniform distribution of initial TRE (iTRE) values between 0 and 20 mm. This distribution of iTREs was achieved by randomly generating a set of transformations, examining the resulting TRE values, and placing these TRE values into separate discrete bins.

Once again, 100 total registrations were performed on each phantom using the proposed method. The results of these registrations are presented in Table 2 with the iTRE vs. final TRE (fTRE) plots of all five patient phantoms found in Fig. 6a–e. Any resulting fTRE values that are above 25 mm were set to 25 mm for purposes of visualization. Registrations were considered as failures for an fTRE value above 3 mm.

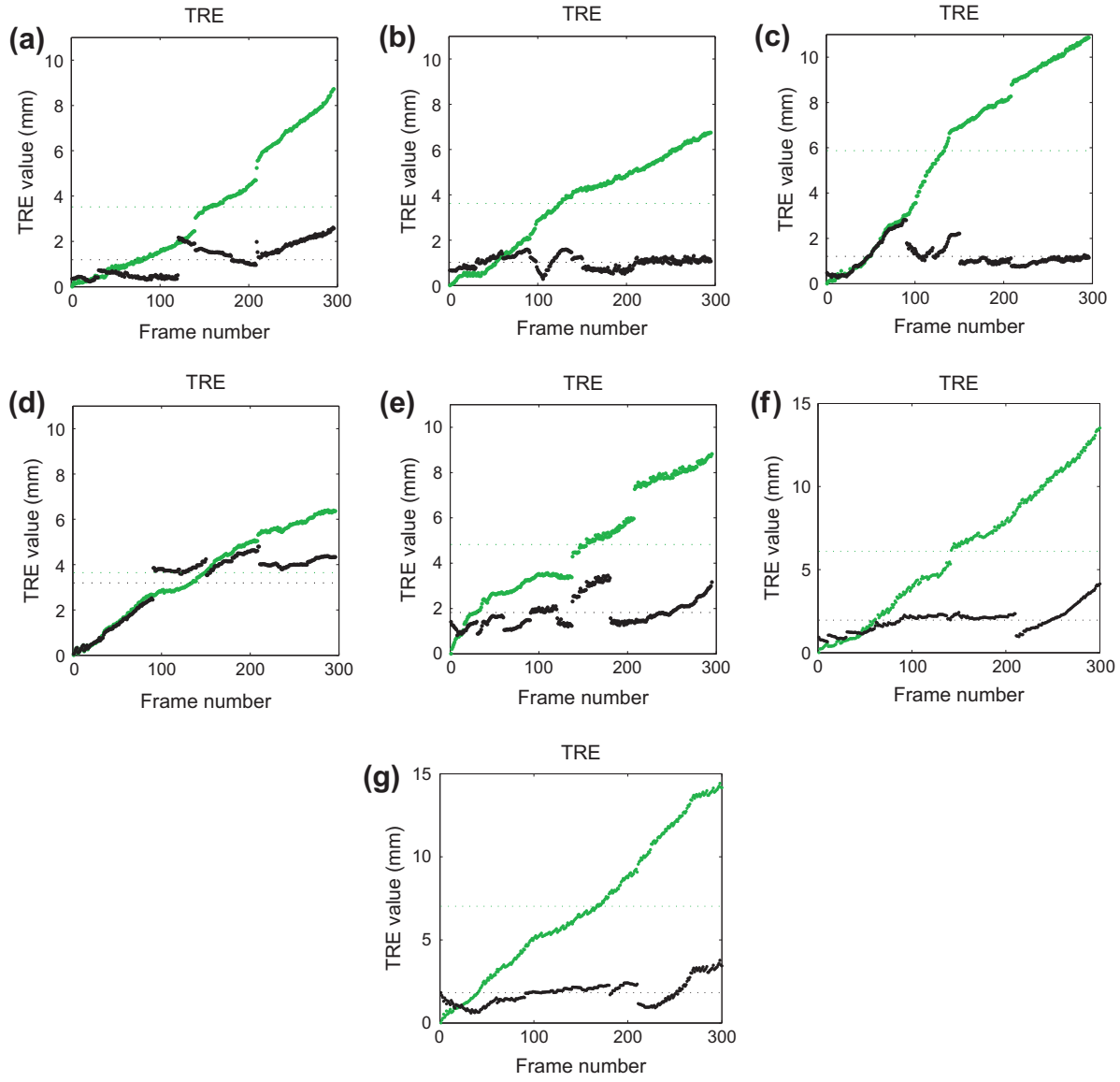

Fig. 4. TRE plots over seven different freehand US scans. Figures (a)–(e) Patient numbers 1–5. Figures (f and g) represent both scans of the lamb cadaver spine. Speckle-tracked results are in lighter color while registrations with CT using the proposed method are in black and the mean TRE values are plotted as horizontal lines of the respective color.

Table 1
TRE of the speckle-tracked US and after registration with CT using the proposed method for each phantom averaged over 100 trials. The initial slices of the US and the CT volumes are aligned prior to registration. The fourth column is the average percentage of frames below 3 mm throughout the final registered volume. The success rate is defined as the percentage of registrations with less than 3 mm TRE.

Phantom number	Speckle-tracked TRE (mm)	Mean registration TRE (mm)	Mean % of frames < 3 mm TRE	Success rate (%)
1	3.52	1.27 ± 0.09	99.9	100
2	3.62	1.11 ± 0.07	100	100
3	5.87	1.18 ± 0.08	99.8	100
4	3.64	3.09 ± 0.26	33.1	30
5	4.82	2.17 ± 0.27	83.6	98

3.2. Animal study

Two tracked freehand US scans were acquired on the surface of the lamb skin, over the lumbar spine region. The process described in Section 3.1 was then followed to align the CT volume with freehand US scans of the spine to the gold standard followed by a rigid registration. These freehand 3D US scans each consist of 300 frames and were acquired on the same lamb spine and subsequently reconstructed using speckle tracking. Both scans were performed over different areas of the spine. Capture range experiments for the lamb data are plotted in Fig. 6f and g.

3.2.1. Speckle tracking and US-to-CT registration

The resulting speckle tracking TRE plots over all frames in each scan are shown in Fig. 4f and g as the lighter color points. We see a significant drift for the speckle-tracked volume, more than that of the patient phantoms. TRE values for the lamb spine experiments can be found in Table 3. These results are very similar to those of the patient phantom experiments. Fig. 4f and g also displays the resulting TREs for an example registration from each of the dataset as black points. Additionally, visual results of the lamb registration can be seen in Fig. 5d–f. Looking at the speckle-tracked reconstruction image, it is clear that the areas of strong reflection, as referenced by the arrows, do not match those in the groundtruth and

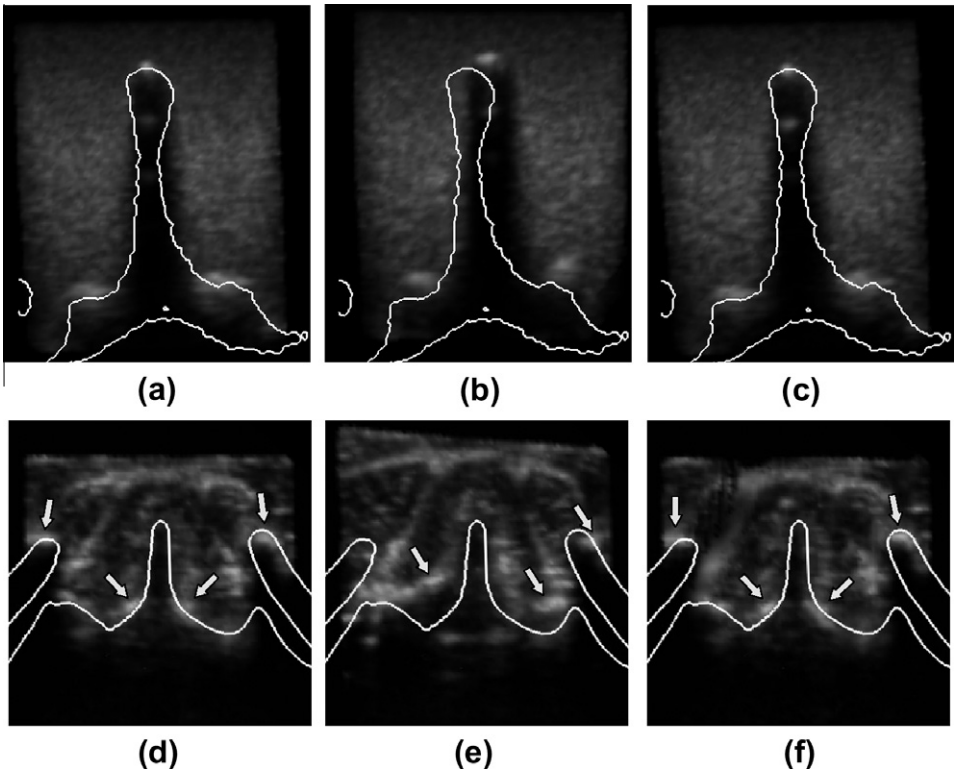

Fig. 5. Top row: A slice from an US reconstruction of the second patient phantom data set with the CT bone surface contour overlaid using positions from (a) ground truth, (b) speckle-tracking, and (c) after correction through registration using the proposed method. Bottom row: A slice from an US reconstruction of the lamb with the CT bone surface contour overlaid using positions from (d) ground truth, (e) speckle tracking, and (f) registration. The arrows show areas of strong reflection in the US. The bone structure on the left and right side of the images above the vertebra represents the overlapping ilium bone of the pelvis.

Table 2
Final TRE of the registered speckle-tracked US volumes after registration with CT for each phantom averaged over 100 trials. The initial slices of the US and the CT volumes are aligned prior to registration. The initial TRE values varied uniformly between 0 and 20 mm in each phantom. The mean TRE value only considers successful registrations, which had final TRE values below 3 mm. Success rate is defined as the percentage of successful registrations out of the 100 trials.

Phantom number	Mean final TRE (mm)	Success rate iTRE (%)	Success rate for iTRE < 10 mm (%)
1	1.82 ± 0.09	92	96
2	1.35 ± 0.07	84	84
3	1.23 ± 0.08	87	98
4	1.83 ± 0.26	96	100
5	1.90 ± 0.27	55	82

registered reconstruction. Due to the elevational drift, the speckle-tracked reconstruction image is significantly misaligned with the CT contour.

3.3. Effect of the registration parameters

One factor that must not be overlooked is the effect of the k, n and α parameters outlined in Section 2.1.3, with k representing the number of frames skipped between sub-volume registrations, n representing the number of frames per sub-volume and α representing the regularization scale. We experimentally determined the range of these parameters.

First, to study the effect of k, its value was varied between 5 and 40 in increments of 5. Two of the phantom datasets and a lamb dataset were registered to their corresponding CT volume for a total of 100 times. Additionally, a value of $n = 60$ was kept constant across all registrations. The average TRE value for each trial is plotted in Fig. 7a.

Next, a series of experiments were performed to examine the effect of n on registration accuracy. The experiments were set up to be identical to those designed above, only the value of n is varied between 30 and 100 in increments of 10. A constant value of $k = 16$ was used. The results are plotted in Fig. 7b.

Finally, we performed experiments to examine the effect of the regularization scale term, α. Again, similar experiments were carried out as those performed above, only this time we used one phantom. In these experiments, values of $k = 16$ and $n = 60$ were used and the value of α was varied from 0 to 0.5 in increments of 0.01. The results are shown in Fig. 7c.

4. Discussion

4.1. Phantom study

4.1.1. Speckle tracking and US-to-CT registration

It is apparent from the results in Table 1 that our registration framework significantly improves the reconstruction of the speckle-tracked US. Drift errors in the speckle-tracked reconstruction were clearly shown. Setting a target of 3 mm as a successful registration, four out of the five patient phantom registrations were successful. Looking at the percentage of frames in each registration that were below this 3 mm threshold, we see that there were greater than 90% of all frames registering below this value for three out of five patient phantoms, with the fourth above 80%. Variations as well as similarities in the spine cause some sub-volumes to register better than others. There especially exists a great deal of similarity in the vicinity of the spinous process between different frames.

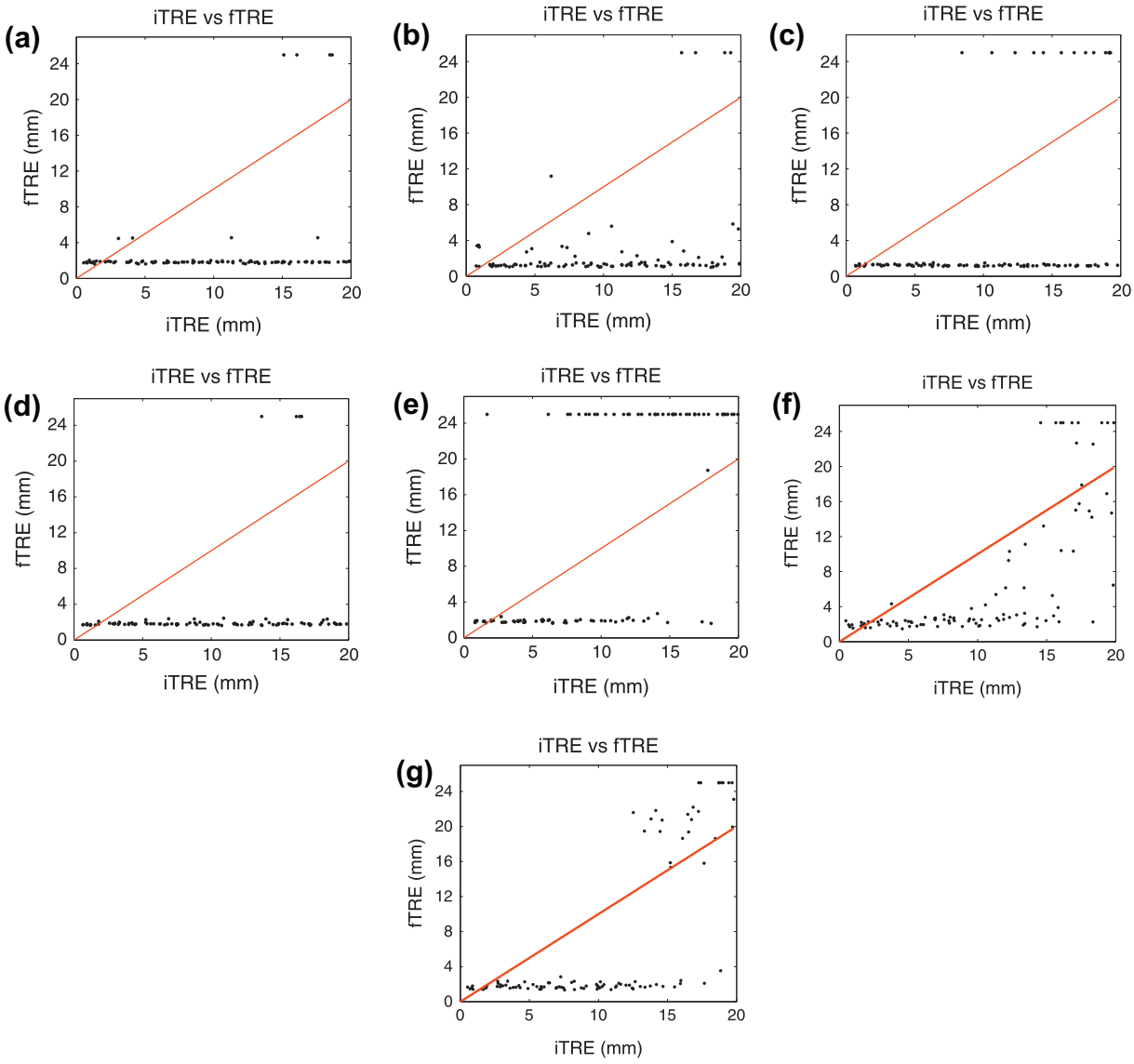

Fig. 6. Plots of the initial TRE values vs. final TRE values over 100 registrations are shown in (a)–(e) for each of the five phantoms, and (f and g) for each of the two lamb datasets.

Table 3
TRE of the speckle-tracked US and after registration with CT for each scan of the lamb spine averaged over 100 trials. The initial slices of the US and the CT volumes are aligned prior to registration. The fourth column is the average percentage of frames below 3 mm throughout the final registered volume.

Scan number	Speckle-tracked TRE (mm)	Mean registration TRE (mm)	Mean % of frames below 3 mm TRE
1	6.10	1.89 ± 0.27	90.3
2	7.03	1.61 ± 0.18	87.8

Looking at the failed registration case of patient 4, we see a reduction in mean TRE of only 15.1%. Fig. 4d shows that the registration had a difficult time diverging away from the speckle-tracked initial position. For this particular case, the regularization term appears to have been too strong, preventing any significant movement in each sub-volume registration. This is the disadvantage of using a regularization term in the registration, as it can overpower the similarity between the US and CT volumes. For this dataset, when the regularization scale was reduced to a value of 0.005, the mean TRE over 100 registrations reduced to 2.51 ± 0.55 with 62.8% of all frames below 3 mm, which is a more acceptable result. The result suggests that further improvement will be necessary to reduce the dependency of the optimization process on the regularization term for clinical translation of the approach.

In Fig. 4 we see some discontinuities in the TRE plots. This behavior can be attributed to the fact that the spinous process begins to disappear at the transition between vertebrae. However, there is still enough information in the absence of the spinous process to register consistently under 3 mm.

4.1.2. Registration capture range

Experiments to determine the capture range of the registration algorithm showed varying levels of success. When studying the success rate for registrations with an iTRE value of less than 10 mm, three of the five phantoms performed well; all above 96% success rate. The other two phantoms both perform above 80%. The majority of the failures in these two cases occurred when the iTRE was above 7 mm. Studying the success rate over the entire 20 mm range, only two of the five phantoms performed above 90% success rate. One of the phantoms performed very poorly with a 55% success rate. This low success rate can possibly be attributed

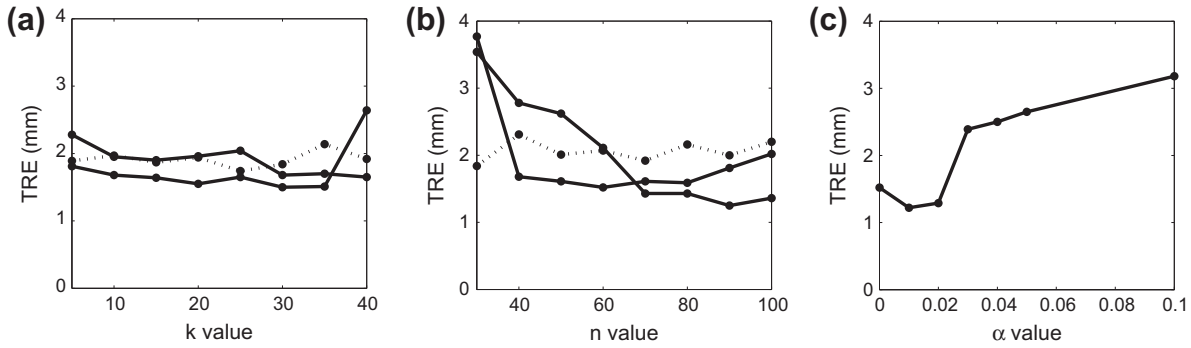

Fig. 7. Plots showing the effect on the TRE of changing (a) the number of frames skipped between each sub-volume registration, k, (b) the number of frames per sub-volume registration, n, and (c) the regularization scale, α. Solid lines represent patient phantom datasets and dotted lines represent the first lamb cadaver dataset.

to a poor initial rigid registration. The speckle-tracked reconstruction was not able to rigidly register with the entire CT volume very well and thus failed before our registration algorithm was able to begin.

The results discussed above point out one particular vulnerability associated with the proposed algorithm. If the US and CT volumes are not in a close initial alignment, they must be rigidly registered together to provide a close initial guess. If this initial rigid registration has a large error, the algorithm will have little chance to compensate for this error. The initial guess is important since the first sub-volume registration sets the course for the rest of the registration.

Large fTRE values (>20 mm) indicate that the US volume and CT volume have drifted entirely away from each other. This drift may occur when the US volume overlaps with the CT volume in an area without bone. Registration to the wrong vertebrae is also a possibility when high iTRE values are used. The complete CT volume contained five vertebrae in the patient phantoms and seven vertebrae in the lamb spine. The speckle-tracked US scans contained at most two vertebrae, so the registration would have several local minima over the entire spine. A potential solution to this problem would be to restart the registration at different locations separated by the distance between vertebrae measured using an initial sagittal imaging scan (Kerby et al., 2008). Also, the inclusion of more than two vertebrae would decrease the number of failures as the additional vertebrae would provide more information for the registration.

4.2. Animal study

Results of the lamb registrations show similarity to those in the phantom studies. The initial speckle-tracked TRE is larger than those of the patient phantom data sets due to the lack of speckle found in the lamb tissue around the vertebrae. Speckle decorrelation correction described in Section 3.2.1 was able to improve the speckle tracking accuracy from 6.93 mm to 6.1 mm in the first scan and from 7.86 mm to 7.03 mm in the second scan. Despite an increase in initial speckle-tracked error as compared to the patient phantoms, the registration was still able to successfully register the lamb US and CT volumes to within 2 mm average TRE, with over 87% of all frames being within the 3 mm TRE threshold. Visually, we see improved results in Fig. 5 where the registered volume is shown to be much closer to the gold-standard than the speckle-tracked volume.

The reason that the patient phantoms and the lamb scans produce similar results is that despite differences in tissue surrounding the vertebrae, the reflections seen at the tissue to bone interface in US are always clearly distinguishable. In the US images, the interface itself will be very bright, due to a large percentage of the US being reflected from the same spot. Additionally, below the interface will have a shadow. The bone surface and underlying shadow are easily able to be matched between the US and simulated US from CT. Any additional surrounding tissue can then be used in the registration to further improve the accuracy, especially in the lamb scans, as the phantoms had little surrounding tissue structure.

It should also be noted that the lamb datasets exhibited some cases of a complete loss of speckle correlation between images due to the inhomogeneity of the tissue. In these cases, the position of the image had to be estimated based on the previous frames as described in Section 2.1.1. This loss of correlation did not prove to be a problem since the loss of speckle correlation was temporary, as a linear, controlled probe motion was used for the experiments. Furthermore, the added information surrounding the bone in the lamb tissue allowed for even more flexibility in the selection of the registration parameters.

4.3. Effect of registration parameters

The effect of k on the registration results of phantom and lamb datasets with their corresponding CT volumes, for a constant value of $n = 60$, is plotted in Fig. 7a. While, a higher value of k results in an overall faster registration, the mean TRE values fail to show significant variation as the value for k is changed. The best TRE value always seems to occur for a k value of between 10 and 30. One explanation for the lack of importance of k in the patient data is that each sub-volume is able to register well, fairly independently of the other sub-volumes. For our final registrations, a value of $k = 30$ was used as it is very close to the best registration accuracy for the phantoms and the lamb spine.

The results of changing the values of n while $k = 16$ are plotted in Fig. 7b. Based on the results of these experiments, we can see that a smaller number of frames used for each sub-volume increases the error in the two phantoms. In the case of using 30 frames, the error was very large as compared with the other values. When fewer frames are used, the registration has less information to work with. A set of about 30 frames corresponds to an elevational scan distance of about 5–10 mm. When looking at US images of the spine within this distance, we see a lot of similarity from frame to frame, as the spinous process does not provide much variation over short distances. Additionally, the tissue surrounding the phantoms was completely homogeneous, providing no additional information. The only information that the registration can work with is the information in the reflection of the bone. In the case of the lamb spine, the problem was different. The US scan of the lamb contains much more information in the surrounding tissue close to the bone, and thus is able to register with higher accuracy when fewer frames are used. There is also an increase in error

for the phantoms as n increases beyond the best value. This increase in error can be attributed to speckle-track becomes increasingly more difficult to register the speckle-tracked US volume when more frames are used. In the end, a value of $n = 80$ was used as a balance between the results from the two phantoms and the lamb cadaver.

The effect of the regularization scale α on registration, with constant values of $k = 16$ and $n = 60$ are shown in Fig. 7c. Larger α values appear to increase the error significantly. The increased error is likely due to the preference given to the speckle-tracked positions over the values of the similarity metric. Since the regularization is determined based on the distance the sub-volume moves, a larger α value shows a preference to maintain the initial position of the speckle-tracking. Using larger α values, the registration error will converge to the speckle-tracked error. Also, we see that a value of $\alpha = 0$ is not the best value, as this will result in each sub-volume being registered independently. Adding the regularization restricts the sub-volume movement from being too extreme.

4.4. Computation time

The computational complexity of the proposed algorithm is relatively high, while the current implementation is not optimized for speed. A single registration takes approximately 15–30 min on an US volume of 300 images, for given values of n and k, on a conventional personal computer. Registration time increases to approximately 1 h when an initial rigid registration is carried out as was done in the capture range experiments. We are currently pursuing a GPU implementation of the proposed technique to alleviate this problem.

5. Conclusion

We presented a technique for simultaneous accurate reconstruction of speckle-tracked freehand 3D ultrasound, and its registration to a CT volume of the same subject. We used the CT of the subject as a global map to compensate for the drift in the speckle-tracked 3D ultrasound data. The proposed method for the registration of CT to speckle-tracked 3D US proves to be straightforward, combining previous works in speckle-tracked reconstruction (Housden et al., 2006) and US-to-CT registration (Wein et al., 2008). The reported registration errors converged to a value consistently below 3 mm in four out of five patient phantoms as well as in the lamb spine. In addition, the drift errors present in the speckle-tracked US data were eliminated by the registration process. Even though the registration algorithm requires a few user-set parameters for speckle-tracked reconstruction and US simulation, the algorithm performance is robust to the value of these parameters. Further research is required to determine the range of acceptable parameters for clinical purposes.

Additional ways in which the proposed registration method could be improved include (1) using more sophisticated approaches to the speckle-tracking problem; (2) multi-resolution registration of US and CT volumes; and (3) real-time implementation of the method for clinical translation.

While we used a straightforward reconstruction method, alternative algorithms proposed in the literature (Housden et al., 2007; Laporte and Arbel, 2008; Rivaz et al., 2007) may be used. These algorithms can potentially generate better initial 3D US volumes for the registration framework, and improve the overall accuracy.

The registration process can be further improved by using multiple sweeps through the volume with each sweep having increasing resolution levels. Additionally, a registration process could be developed in which the characteristics of the speckle and the drift errors are modelled and incorporated. Unfortunately, these models are very difficult to derive due to the inhomogeneity of different tissues. Even still, unexpected probe motions due to hand jitter and patient motion may still be difficult for the model to maintain accuracy.

The current implementation of our technique is slow, as the implementation speed was not a focus of this work. A sufficiently fast implementation is desired for clinical use. GPU implementation of the US simulation from CT (Shams et al., 2008; Kutter et al., 2009) is an active area of research that our research group is currently also pursuing.

The proposed registration method shows promise for clinical applications. In a clinical setting, an initial freehand US sweep across the spine of the patient would be acquired in a slow, controlled manner. As there are some limitations with the speckle tracking, image acquisition protocols pertaining to the probe speed, probe motion and patient motion among other things should be in place to ensure that a useful volume is acquired. If the reconstructed US volume can be successfully registered to the preoperative CT volume, the approach could be used to provide a threedimensional context for the percutaneous spinal intervention procedure.

Acknowledgments

This work was jointly funded by the Natural Sciences and Engineering Research Council (NSERC) and the Canadian Institutes of Health Research (CIHR). Dr. Gabor Fichtinger was supported as a Cancer Ontario Research Chair. The authors would also like to thank the assistance provided by Dr. Dan Borshneck, Dr. David Pichora and Dr. Manuela Kunz, as well as the staff at the Kingston General Hospital, throughout this research.

References

Arun, K.S., Huang, T.S., Blostein, S.D., 1987. Least-squares fitting of two 3-D point sets. IEEE Transactions on Pattern Analysis and Machine Intelligence 9 (5), 698–700.

Barratt, D.C., Penney, G., Chan, C.S., Slomczykowski, M., Carter, T.J., Edwards, P.J., Hawkes, D.J., 2005]. Self-calibrating ultrasound-to-CT bone registration. In: Medical Image Computing and Computer Assisted Intervention. Lecture Notes in Computer Science, vol. 3749. Springer, pp. 605–612.

Besl, P., McKay, H., 1992]. A method for registration of 3-D shapes. IEEE Transactions on Pattern Analysis and Machine Intelligence 14 (2), 239–256.

Chen, J.F., Fowlkes, J.B., Carson, P.L., Rubin, J.M., 1997]. Determination of scan-plane motion using speckle decorrelation: theoretical considerations and initial test. International Journal of Imaging Systems and Technology 8 (1), 38–44.

Chen, T.K., Abolmaesumi, P., Thurston, A.D., Ellis, R.E., 2006]. Automated 3D freehand ultrasound calibration with real-time accuracy control. In: Medical Image Computing and Computer Assisted Intervention – MICCAI 2006. Lecture Notes in Computer Science, vol. 4190. Springer, pp. 899–906.

Datta, S., Lee, M., Falco, F.J., Bryce, D.A., Hayek, S.M., 2009]. Systematic assessment of diagnostic accuracy and therapeutic utility of lumbar facet joint interventions. Pain Physician 12, 437–460.

Fenster, A., Downey, D.B., Cardinal, H.N., 2001]. Three-dimensional ultrasound imaging. Physics in Medicine and Biology 46 (5), R67–R99.

Fitzpatrick, J., West, J., Maurer, C.R., 1998]. Predicting error in rigid-body point-based registration. IEEE Transactions on Medical Imaging 17 (5), 694–702.

Gee, A.H., Housden, R.J., Hassenpflug, P., Treece, G.M., Prager, R.W., 2006]. Sensorless freehand 3D ultrasound in real tissue: speckle decorrelation without fully developed speckle. Medical Image Analysis 10 (2), 137–149.

Gill, S., Mousavi, P., Fichtinger, G., Pichora, D., Abolmaesumi, P. 2009a. Group-wise registration of ultrasound to CT images of human vertebrae. In: Proceedings of SPIE Medical Imaging: Visualization, Image-Guided Procedures, and Modeling, vol. 7261. Lake Buena Vista, FL, USA, p. 72611O.

Gill, S., Mousavi, P., Fichtinger, G., Boisvert, J., Chen, E., Pichora, D., Abolmaesumi, P., 2009b]. Biomechanically constrained groupwise US to CT registration of the lumbar spine. In: Medical Image Computing Computer Assisted Intervention. Lecture Notes in Computer Science, vol. 5761. Springer, pp. 803–810.

Hansen, N., 2006]. The CMA evolution strategy: a comparing review. In: Lozano, J.A., Larranaga, P., Inza, I., Bengoetxea, E. (Eds.), Towards a New Evolutionary Computation, Advances on Estimation of Distribution Algorithms. Springer, pp. 75–102.

Hassenpflug, P., Prager, R.W., Treece, G.M., Gee, A.H., 2005]. Speckle classification for sensorless freehand 3D ultrasound. Ultrasound in Medicine and Biology 31 (11), 1499–1508.

Herring, J., Dawant, B., Maurer, C.R., Muratore, D., Galloway, R., Fitzpatrick, J., 1998]. Surface-based registration of CT images to physical space for image-guided surgery of the spine: a sensitivity study. IEEE Transactions on Medical Imaging 17 (5), 743–752.

Housden, R.J., Gee, A.H., Treece, G.M., Prager, R.W., 2006]. Subsample interpolation strategies for sensorless freehand 3D ultrasound. Ultrasound in Medicine and Biology 32 (12), 1897–1904.

Housden, R.J., Gee, A.H., Treece, G.M., Prager, R.W., 2007]. Sensorless reconstruction of unconstrained freehand 3D ultrasound data. Ultrasound in Medicine and Biology 33 (3), 408–419.

Housden, R., Treece, G., Gee, A., Prager, R., 2008a]. Calibration of an orientation sensor for freehand 3D ultrasound and its use in a hybrid acquisition system. BioMedical Engineering OnLine 7 (1), 5.

Housden, R., Gee, A.H., Prager, R.W., Treece, G.M., 2008b]. Rotational motion in sensorless freehand three-dimensional ultrasound. Ultrasonics 48 (5), 412–422.

Kerby, B., Rohling, R., Nair, V., Abolmaesumi, P. 2008. Automatic identification of lumbar level with ultrasound. In: IEEE Engineering in Medicine and Biology, pp. 2980–2983.

Krupa, A., Fichtinger, G., Hager, G. 2007. Full motion tracking in ultrasound using image speckle information and visual servoing. In: IEEE International Conference on Robotics and Automation, Roma, Italy, pp. 2458–2464.

Kutter, O., Shams, R., Navab, N., 2009]. Visualization and GPU-accelerated simulation of medical ultrasound from CT images. Computer Methods and Programs in Biomedicine 94 (3), 250–266.

Lang, A., Mousavi, P., Fichtinger, G., Abolmaesumi, P. 2009. Fusion of electromagnetic tracking with speckle-tracked 3D freehand ultrasound using an unscented Kalman filter. In: Proceedings of SPIE Medical Imaging: Visualization, Image-Guided Procedures, and Modeling, vol. 7265. Lake Buena Vista, FL, USA, p. 72651A.

Laporte, C., Arbel, T., 2008]. Combinatorial and probabilistic fusion of noisy correlation measurements for untracked freehand 3D ultrasound. IEEE Transactions on Medical Imaging 27 (7), 984–994.

Madsen, E.L., Hobson, M.A., Shi, H., Varghese, T., Frank, G.R., 2005]. Tissue-mimicking agar/gelatin materials for use in heterogeneous elastography phantoms. Physics in Medicine and Biology 50 (23), 5597–5618.

Moghari, M.H., Abolmaesumi, P., 2005]. A novel incremental technique for ultrasound to CT bone surface registration using unscented Kalman filtering. In: Medical Image Computing and Computer Assisted Intervention. Lecture Notes in Computer Science, vol. 3750. Springer, pp. 197–204.

Muratore, D.M., Russ, J.H., Dawant, B.M., Robert, J., Galloway, L., 2002]. Three-dimensional image registration of phantom vertebrae for image-guided surgery: A preliminary study. Computer Assisted Surgery 7 (6), 342–352.

Penney, G., Barratt, D., Chan, C., Slomczykowski, M., Carter, T., Edwards, P., Hawkes, D., 2006]. Cadaver validation of intensity-based ultrasound to CT registration. Medical Image Analysis 10 (3), 385–395.

Rivaz, H., Zellars, R., Hager, G., Fichtinger, G., Boctor, E. 2007. Beam steering approach for speckle characterization and out-of-plane motion estimation in real tissue. In: Proceedings of IEEE International Ultrasonics Symposium, pp. 781–784.

Shams, R., Hartley, R., Navab, N., 2008]. Real-time simulation of medical ultrasound from CT images. In: Medical Image Computing and Computer Assisted Intervention. Lecture Notes in Computer Science, vol. 5242. Springer, pp. 734–741.

Tuthill, T., Krucker, J., Fowlkes, J., Carson, P., 1998]. Automated three-dimensional US frame positioning computed from elevational speckle decorrelation. Radiology 209 (2), 575–582.

Wein, W., Brunke, S., Khamene, A., Callstrom, M., Navab, N., 2008]. Automatic CT-ultrasound registration for diagnostic imaging and image-guided intervention. Medical Image Analysis 12, 577–585.

Weng, L., Tirumalai, A., Lowery, C., Nock, L., Gustafson, D., Von Behren, P., Kim, J., 1997]. US extended-field-of-view imaging technology. Radiology 203 (3), 877–880.

Winter, S., Brendel, B., Pechlivanis, I., Schmieder, K., Igel, C., 2008]. Registration of CT and intraoperative 3-D ultrasound images of the spine using evolutionary and gradient-based methods. IEEE Transactions on Evolutionary Computation 12 (3), 284–296.

Yushkevich, P.A., Piven, J., Cody Hazlett, H., Gimpel Smith, R., Ho, S., Gee, J.C., Gerig, G., 2006]. User-guided 3D active contour segmentation of anatomical structures: significantly improved efficiency and reliability. Neuroimage 31 (3), 1116–1128.